University of Cologne
Institute of Physics II

Bachelor Thesis

Raman Scattering Spectroscopy of Orbital Order in Epitaxial Vanadate Films

Date of Submission: 07.06.2016

Author: Lena Bussmann

Supervisor: Dr. Ionela Lindfors-Vrejoiu

1st examiner: Prof. Dr. Paul H. M. van Loosdrecht

2nd examiner: Prof. Dr. Markus Grüninger

Contents

1 Investigation of Orbital-Ordered $LaVO_3$ Epitaxial Films by Raman Scattering Spectroscopy: Background and Theory

The following chapter is meant to elucidate the fundamental motivation of research in the field of thin films and specify the structural and physical properties of the investigated material $LaVO_3$. In particular, it will address the characteristics of the spin- and orbital-ordered states in this crystal.

1.1 Introduction: Motivation of the Ongoing Research on Vanadate Thin Films

Transition metal oxide compounds have been studied intensively during the last years, as many of them exhibit rich phase diagrams with long-range ordered as well as disordered states and complex physical properties, such as Mott transitions or colossal magnetoresistance. $LaVO_3$ is a member of this group which has often been investigated. In spite of the high number of experiments and theoretical studies to enlighten the complex physics in transition metal oxides, many details are still not understood to full satisfaction.

It has been shown that $LaVO_3$ develops a long-range orbital occupation pattern below a certain temperature. Furthermore, orbital-ordered states might allow the observation of collective orbital excitations, so called orbitons. These excitations have often been adressed theoretically by various approaches, but unambiguous experimental evidence is rather difficult. Among other authors, Miyasaka *et al.* [9] [10], who have investigated $LaVO_3$ and related compounds in great detail, claim that it is possible to observe them in $LaVO_3$ using Raman scattering spectroscopy, however, this interpretation is not generally accepted. Studying these rather exotic excitations makes $LaVO_3$ and related compounds interesting candidates for further research.

While the occurrence of orbital order was experimentally investigated and accounted for primarily in $LaVO_3$ single crystals, it is an interesting question if or to which extent these properties are preserved if dimensions or internal structure are changed. In order to study the influence of dimensionality, epitaxial strain and substitution, two samples of $LaVO_3$ epitaxial films grown on different substrates ($(LaAlO_3)_{0.3}(Sr_2TaAlO_6)_{0.7}$ (LSAT) and $DyScO_3$) as well as one $La_{0.75}Sr_{0.25}VO_3$ film grown on LSAT were investigated by Raman scattering spectroscopy. Research on thin films is of great relevance as nanotechnology and thin films are the key elements in nowadays technological advances.

1.2 Crystal Structure, Electronic Configuration and Ordered States in $LaVO_3$

At room temperature, the perovskite-like $LaVO_3$ single crystal is a member of the orthorhombic *Pnmb* space group due to distortions in the form of tilted VO_6 octahedra and displaced La ions, as shown in Fig. 1.

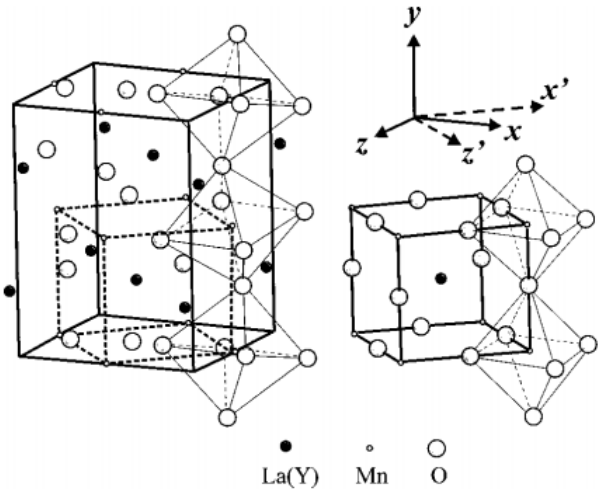

Figure 1: Unit cell of orthorhombic ABO_3. Various compounds ($LaMnO_3$/$YMnO_3$ in this case) belong to this structure type, $LaVO_3$ among them. The simple perovskite cubic structure is shown (right) and, for comparison, the distorted *Pnmb* unit cell with tilted BO_6 octahedra. [7].

Due to the V^{+3} ion, $LaVO_3$ has a $3d^2$ electronic configuration with two electrons in the $3d$ shell. According to crystal field theory, the electron density is not evenly distributed and forms orbitals shaped by the Coulomb potential of the respective lattice symmetry. In a cubic crystal field, the $3d$ shell degeneracy is lifted to form an energetically upper lying e_g orbital and a t_{2g} lower lying one. In the tetragonal symmetry of an orthorhombic lattice, the t_{2g} orbital is further split into xy, xz and yz orbitals. The shape of the orbitals is shown in Fig. 2. The e_g orbitals are not occupied in $LaVO_3$ [11].

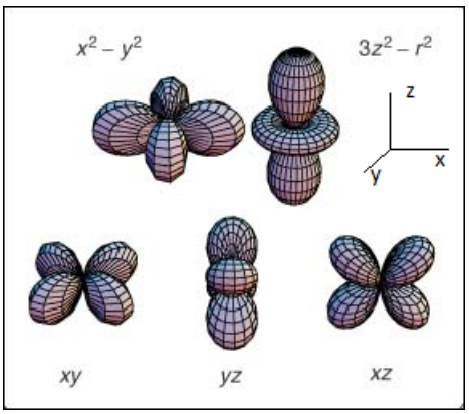

Figure 2: In a cubic crystal field the degeneracy of d orbitals is lifted. The energy of the e_g orbitals ($x^2 - y^2$ and $3z^2 - r^2$) is higher than the t_2g subgroup (xy, yx, zy) because the lobes of e_g orbitals at the transition metal B point toward the negative O ions in the BO_6 octahedra, whereas the t_{2g} orbitals point in between. [6]

The xy orbital is the energetically lowest orbital and therefore occupied permanently by one of the electrons [9]. The localization of the other one is regarded as a further degree of freedom in the crystal system. The question occurs if it is possible to observe a long-range occupation pattern. This phenomenon is called orbital order (OO), in analogy to a regular spin order (SO).

The room temperature phase of $LaVO_3$ single crystals is characterized by an orthorhombic lattice with constants $a = 5.555\,\text{Å}$, $b = 5.553\,\text{Å}$ and $c = 7.849\,\text{Å}$ ($a \approx b \approx \frac{c}{\sqrt{2}}$) [1] and paramagnetic behaviour. At $T_{SO} = 143\,K$, $LaVO_3$ undergoes a magnetic phase transition from a paramagnetic to an antiferromagnetic state. The onset of the SO state is followed by a structural phase transition from orthorhombic $Pbnm$ to monoclinic $P2_1/b$ symmetry at $T = 141\,K$ [10]. The monoclinic lattice constants are $a = 5.59\,\text{Å}$, $b = 5.56\,\text{Å}$ and $c = 7.76\,\text{Å}$ with an angle $\alpha = 90.13°$ [1]. The structural phase transition is accompanied by the development of OO in an alternating d_{yz}/d_{zx} pattern [11]. These spin and orbital order patterns are called C-type and G-type, respectively. They are schematically illustrated in Fig. 3.

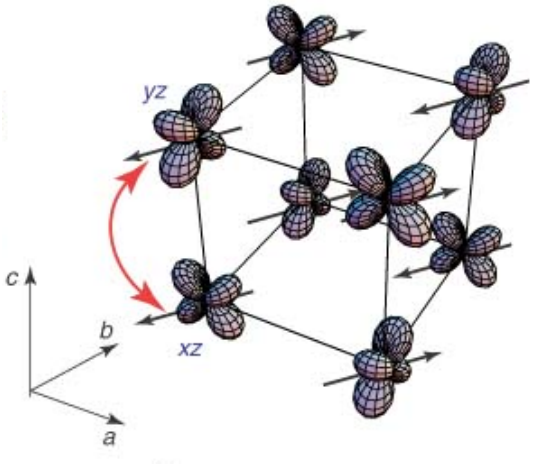

Figure 3: Orientation of occupied t_{2g} orbitals in the magnetic C (orbital G) type low-temperature structure of $LaVO_3$. ($S = 1$ spins are indicated by black arrows.) For the C phase a doubleside arrow indicates the fluctuating orbital occupation between $a = yz$ and $b = xz$ orbitals along the c direction. A second vanadium t_{2g} electron occupies the xy orbital at each vanadium ion and is not shown. [6]

It has been shown that many $R\mathrm{VO}_3$ compounds, similar to $LaVO_3$, undergo magnetic as well as structural phase transitions accompanied by the onset of orbital order [9] [11]. Fig. 4 puts the phase properties of $LaVO_3$ into a comparable context with other compounds of the rare earth metal series. The phase transition temperatures depend on the R-site ionic radius.

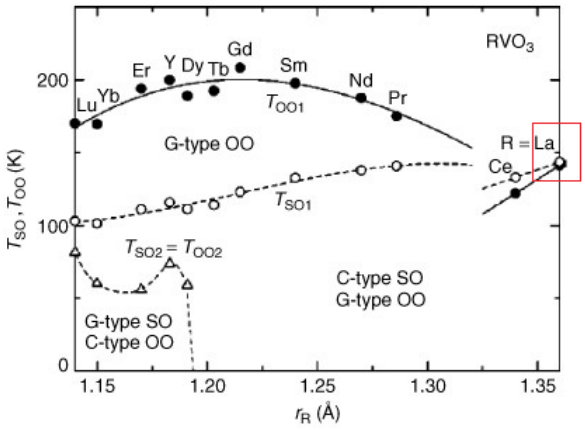

Figure 4: Spin-orbital phase diagram of $R\mathrm{VO}_3$ (R = Lu–La) as function of the cation size r_R. Closed and open circles indicate G-type orbital ordering temperature T_{OO1} and C-type spin ordering T_{SO1}, respectively. Triangles indicate G-type spin (C-type orbital) ordering temperature $\mathrm{T}_{SO2} = \mathrm{T}_{OO2}$. [6]

With growing radius, where the La radius is maximum, the Jahn-Teller distortion as well as the deviation from the V-O-V bond angles gradually decreases. This seems to be the reason for decreased spin and orbital exchange interactions between the nearest-neighbour V sites, hence the ordering sequence changes [9]. In $LaVO_3$ and $CeVO_3$ SO develops primarily followed by OO, while the opposite holds for $PrVO_3$ to YVO_3.

The SO and OO states in $LaVO_3$ can be significantly affected by doping, i. e. the partial substitution of the lanthanum ions by strontium.

1.2.1 Properties of $La_{1-x}Sr_xVO_3$ with a Sr Concentration $x = 0.25$

Substitution in ABO_3 perovskite compounds can be done on both A- and B-site and most often leads to significantly changed structure and properties the parent crystal.

The investigation of $La_{1-x}Sr_xVO_3$ ($0 \leq x \leq 1$) by Inaba *et al.* [8] indicated a structural change from orthorhombic in the $x \leq 0.2$ region to rhombohedral for $x \geq 0.3$, whereas it is difficult to make an unambiguous statement concerning the area in between, where the compound appears to be in a phase-mixed state, propably due to inhomogeneities. In addition, while pure $LaVO_3$ is a Mott Insulator and $SrVO_3$ a metal, a mixed compound $La_{1-x}Sr_xVO_3$ ($0 \leq x \leq 1$) exhibits an metal-insulator transition around $x = 0.18$. The structural and magnetic phase transitions are observable up to a concentration level $x \approx 0.26$. At higher values, it behaves lika a paramagnetic metal (cf. Fig. 5). When the Sr concentration is lower, it undergoes a phase transition from paramagnetic to antiferromagnetic, orbital-disordered metal until $x \approx 0.18$ and from paramagnetic to antiferromagnetic orbital-ordered insulator below [10].

x	T_N (K)
0	144
0.05	126
0.10	110
0.15	95
0.20	75
0.22	20
0.25	
0.28	

(a)

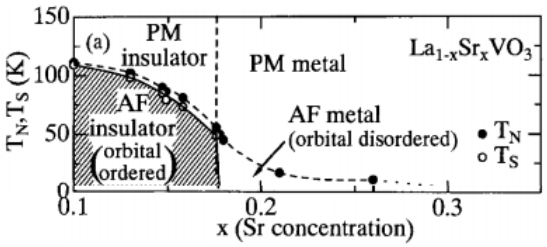

(b)

Figure 5: a)The magnetic phase transition temperature for different x in $La_{1-x}Sr_xVO_3$. The measurements were carried out by a SQUID magnetometer. T_N denotes the Néel temperature, T_S the structural PT temperature. [8] b) Electronic phase diagram of $La_{1-x}Sr_xVO_3$. [10]

We studied a sample with a concentration level $x = 0.25$. According to the phase diagram 5b), orbital order should not be persistent any more at this point and the structural and magnetic transition temperatures are significantly decreased. Fujioka *et al.* [3] have performed Raman measurements on $Nd_{1-x}Sr_xVO_3$ for concentration levels $x = 0, 0.07$ and 0.12. $SrVO_3$ is a cubic perovskite which belongs to the point group symmetry of O_h, which is "Raman forbidden", namely it has no Raman-active phonon modes. Therefore, the experimental results tell us that by Sr-substitution the crystal symmetry actually changes from the orthorhombic distorted perovskite ($NdVO_3$) to the cubic perovskite ($SrVO_3$).

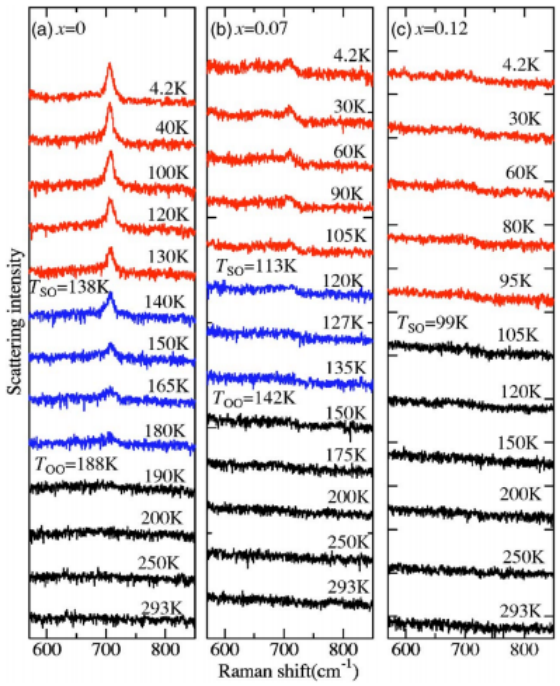

Figure 6: Temperature-dependent Raman spectra of $Nd_{1-x}Sr_xVO_3$ in xx polarization configuration (x represents the nearest-neighboring V-V direction of the ab plane). With increasing strontium concentration level, the orbital ordering related phonon around $700\,cm^{-1}$ disappears. [3]

The Raman data presented in Fig. 6 clearly shows the instability of the orbital ordered phase towards growing doping levels for $Nd_{1-x}Sr_xVO_3$. The properties of $NdVO_3$ are comparable to $LaVO_3$ as it has the same $3d^2$ electronic configuration due to the V^{3+} system. Small residues of the phonon in the Raman spectrum at $x = 0.12$ incidate a not fully concluded phase transition towards an orbital-disordered state, supporting the propositions of Inaba *et al.* [8]. Fujioka *et al.* [3] suggest that short-range orbital order is still persistent at this point.

2 Experimental Approach

The properties and phases in pure and strontium doped epitaxial films can be investigated in a relatively convenient way by Raman scattering spectroscopy. This technique is suitable to observe the transition from orthorhombic to monoclinic symmetry and the corresponding orbital order in $LaVO_3$. A brief introduction into Raman scattering as well as technical details concerning the experimental setup and the samples will be given in greater detail in the following chapter.

2.1 Principles of the Raman Process

If light or electromagnetic radiation in general interacts with a molecule or a solid, most of the incident photons are scattered elastically. The molecule or crystal is being excited to a virtual state and relaxes back to the initial state. The relaxation results in the emission of a photon of same wavelength as the excitation photon. This process without a resulting energy shift is called Rayleigh scattering.

However, under certain conditions, very few photons are also scattered inelastically, while the laws of energy and momentum conservation are obeyed. The final state of the inelastically interacting photon is either higher or lower (the corresponding energy shift is then called Stokes or anti-Stokes shift, respectively) than the initial one. Under room temperature conditions, most molecules are in the ground state and the frequency of occurrence of these interaction processes depend on the population number of the respective state - hence the intensity of anti-Stokes peaks is in general considerably lower than the intensity of Stokes peaks. The different processes are schematically illustrated in Fig. 7.

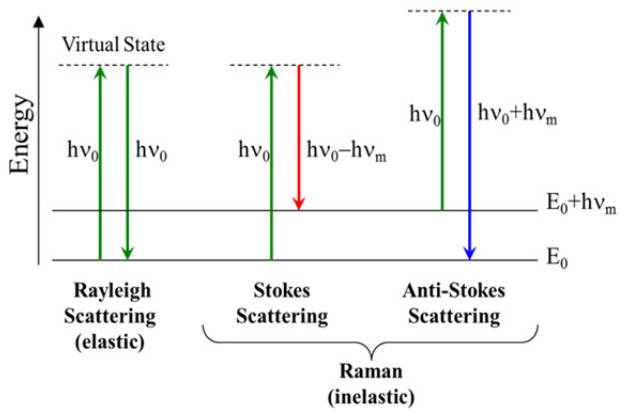

Figure 7: Schematic overview of different scattering processes. The virtual state is not necessarily a real state of the molecule, but the Raman cross section and thus the observable signal is potentially enhanced by several orders of magnitude if the excitation energy lies within a relatively close range of an actual electronic transition energy. [20]

Raman scattering spectroscopy makes use primarily of the inelastically scattered photons that have interacted with matter, in order to derive information about the matter. The yielded information is chiefly related to the structure of matter but also to collective electronic excitation processes. The Raman shift is typically given in wavenumbers, but sometimes also in energy units of meV (according to the relation $E = hc\overline{\nu}$):

$$\overline{\nu} = \frac{1}{\lambda_{incident}} - \frac{1}{\lambda_{scattered}}, [\mathrm{cm}^{-1}/\mathrm{meV}]$$

As a first, simplified approach, this frequency change of the scattered light with respect to the incident light originates in its interaction with electrons and lattice. The incident photons interact with the lattice vibrational modes or phonons in a way depending on the specific phonon symmetry and on the properties of the incident light (wavelength, polarization). This results in the local deformation of the electron shell and therefore in the change of dielectric susceptibility. Note that this does not necessarily mean a change in the overall electric dipole moment of a molecule as a consequence of a change of atomic positions, on which IR spectroscopy is based.

In a crystal lattice, the dielectric susceptibility is a tensor χ, expressed as a Taylor series around the lattice equilibrium position. This position is represented by the lattice displacement or rather the oscillation normal coordinate $\boldsymbol{Q}(\boldsymbol{r}, t)$, a function of the respective phonon wave vector $\boldsymbol{k}$, its direction and frequency. The scattering process is Raman

active, if the first derivative term of the dielectric susceptibility tensor is non-vanishing:

$$\chi(\boldsymbol{k}, \omega, \boldsymbol{Q}) = \chi_0(\boldsymbol{k}, \omega) + \left(\frac{\partial \chi}{\partial Q}\right)_0 \boldsymbol{Q}(\boldsymbol{r}, t) + \dots \tag{1}$$

The first term corresponds to the Rayleigh scattering, while the second one respresents Raman processes.

This expression is expanded to the so called Raman tensor $\boldsymbol{R} = \frac{d\chi}{d\boldsymbol{Q}}\hat{\boldsymbol{Q}}$, introducing a unit vector $\hat{\boldsymbol{Q}} = \frac{Q}{|Q|}$. This tensor is associated with the resulting Raman intensity [1]:

$$I_R \propto I_I |\boldsymbol{e_i} \cdot \boldsymbol{R} \cdot \boldsymbol{e_s}|^2 \tag{2}$$

I_I is the incident light (laser) intensity and $\boldsymbol{e_i}$ and $\boldsymbol{e_s}$ denote the polarization direction of the incident and scattered light which can be adjusted experimentally Structural properties as well as orientation in an anisotropic lattice yield important information in terms of developing a suitable experimental setup, which is being adressed in greater detail in 2.3.

Point group analysis allows to classify crystals with regard to their lattice symmetry. The Raman tensor provides selection rules determining which lattice vibration modes are either Raman active or "forbidden" by symmetry, i.e., the tensor elements $\alpha_{ij} \neq 0$ can possibly be observed by Raman spectroscopy.

As it is predominantly based on lattice vibrational modes and their specific symmetry, Raman spectroscopy is a suitable technique to detect lattice alterations induced by distortions or phase transitions.

2.2 Raman Spectra of Pure $LaVO_3$ Single Crystals

Raman scattering spectroscopy was performed in great detail on $LaVO_3$ single crytals by Miyasaka *et al.* [11] [9] in different excitation wavelengthes and polarization configurations.

The polarization geometry is given in the notation $k_i\,(e_i e_s)\,k_s$, $k_{i/s}$ denotes the propagation direction of incident and scattered light and $e_{i/s}$ the respective polarization. The optical axes x, y, and z correspond to the orthorhombic crystal axes $a+b$, $a-b$ and c and approximately go along with the directions of the V-O-V bondings [9].

[1] Equations taken from [21]

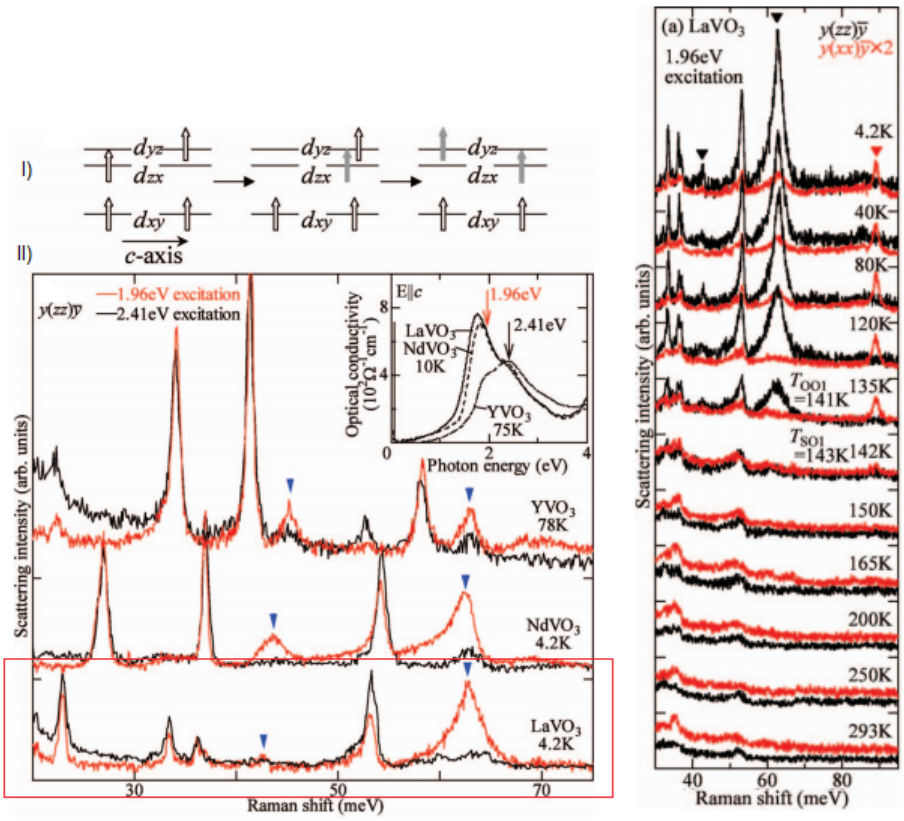

(a) (b)

Figure 8: a) II) Raman scattering spectra at 4.2 K in $LaVO_3$ (red box); the inset presents optical conductivity spectra at 10 K in $LaVO_3$ and the peak representing the Mott-Hubbard gap transition. The blue arrows indicate the peaks that show resonant enhancement with the Mott-Hubbard gap energy ($\approx$ 2 eV) when using the excitation laser energy 1.9 eV. They are assigned to the two-orbiton mode. The two-orbiton process is sketched in I). b) Polarization dependence of the $LaVO_3$ Raman spectrum for an excitation energy 1.96 eV. [9].

Fig. 8 shows the Raman spectra of $LaVO_3$ depending on excitation wavelength on the one and polarization configuration on the other hand. The peaks around 350 cm^{-1} and 511 cm^{-1} or 43 meV and 62 meV, respectively, show significant enhancement with an excitation energy 1.96 eV. According to the optical conductivity data (cf. Fig. 8a)II), inset), this energy corresponds to the Mott-Hubbard transition energy around 2 eV. The same holds for the peak at 720 cm^{-1}/89 meV. This dependency points to the involvement of the Mott-Hubbard gap transition as the intermediate state of the two-orbiton process (Fig. 8 a)I)). While the d_{xy} orbital is always occupied, the second electron can hop along the c-axis between the d_{zx} and d_{yz}. On the other hand, the modes also depend on the polarization configuration, as shown by Fig. 8(b)). The peak at 89 meV/720 cm^{-1}

occurs below T_{OO} only in $y(xx)\overline{y}$ configuration whereas the presumed two-orbitons are only visible in $y(zz)\overline{y}$ configuration.

The Raman active phonons of $LaVO_3$ are assigned by comparison with $LaMnO_3$ according to Iliev *et al.* [7].

Table 1: Assigment of the Raman active modes in $LaVO_3$

Wavenumber[cm^{-1}]	Energy[meV]	Origin
182	23	VO_6 Octahedra Rotation
271	34	Oxygen Bending Mode (A_g)
297	37	Phonon (A_g)
350	43	Unclear (Two-Orbiton)
428	53	Jahn-Teller Mode (A_g)
487	60	Phonon (A_g)
511	63	Unclear (Two-Orbiton/B1g(2) Mode)
700	87	Phonon Density of States
720	89	B1g(1) Phonon (orth.)/Oxygen Stretching Mode (A_g)(monocl.)

As indicated in table 1, the origin of particularly the modes at 350 and 511 cm^{-1} is not fully clear yet. Miyasaka *et al.* assigned them to collective electronic (two-orbiton) excitations [9], whereas other authors question this interpretation in favor of a Jahn-Teller phonon origin(cf. Sugai *et al.* [18], who assign the mode around 500 cm^{-1} to the Jahn-Teller phonon and the 350 cm^{-1} mode to a one-orbital wave peak) or a multi-phonon process (cf. Grüninger *et al.* [5] for $LaMnO_3$). Whichever underlying process they originate from, their appearance is associated with the G-type orbital-ordered phase. The 428 cm^{-1} peak, assigned to a Jahn-Teller phonon, seems to be coupled to the orbital excitation as their simultaneous enhancement implies [11].

Raman spectroscopy therefore can potentially provide essential information required to enlighten the origin of excitation processes. It is not only sensitive to lattice modifications but can simultaneously reveal crucial dependencies in terms of polarization or resonance. It is a selective measurement in this respect.

However, it is obviously difficult to prove further and unambiguous evidence concerning the debate about orbital excitations, particularly in the case of thin films where the signal is relatively weak and potentially suffering from an underlying substrate (see 2.4). A further approach could be Raman measurements under applied magnetic field. This could bring additional support to the question if the peaks at 350 and 511 cm^{-1} actually originate from a collective electronic excitation or not.

2.3 The Micro-Raman Experimental Setup

The measurements were performed in the group of Dr. Cameliu Himcinschi, at TU Bergakademie, Institute für Theoretische Physik. The spectra in a range from room temperature to 90 K were recorded in backscattering geometry using a JobinYvon LabRAM HR800 Raman spectrometer. Backscattering geometry means that the direction of propagation of both incident and scattered laser beam was perpendicular to the sample surface.

Fig. 9 shows the basic setup in Freiberg. The chosen excitation laser was a HeNe with 633 nm wavelength, which is equivalent to an energy of 1.96 eV; as described in 2.2, Miyasaka *et al* found some modes in $LaVO_3$ to be resonantly enhanced using this laser energy [9]. The laser power (measured under the microscope objective) was about $P = 1.9\,\mathrm{mW}$ during the whole spectrum acquisition time; it was possible to obtain clearly visible signals but concomitantly avoid the risk of burning the sample or affect its properties by laser-induced thermal effects.

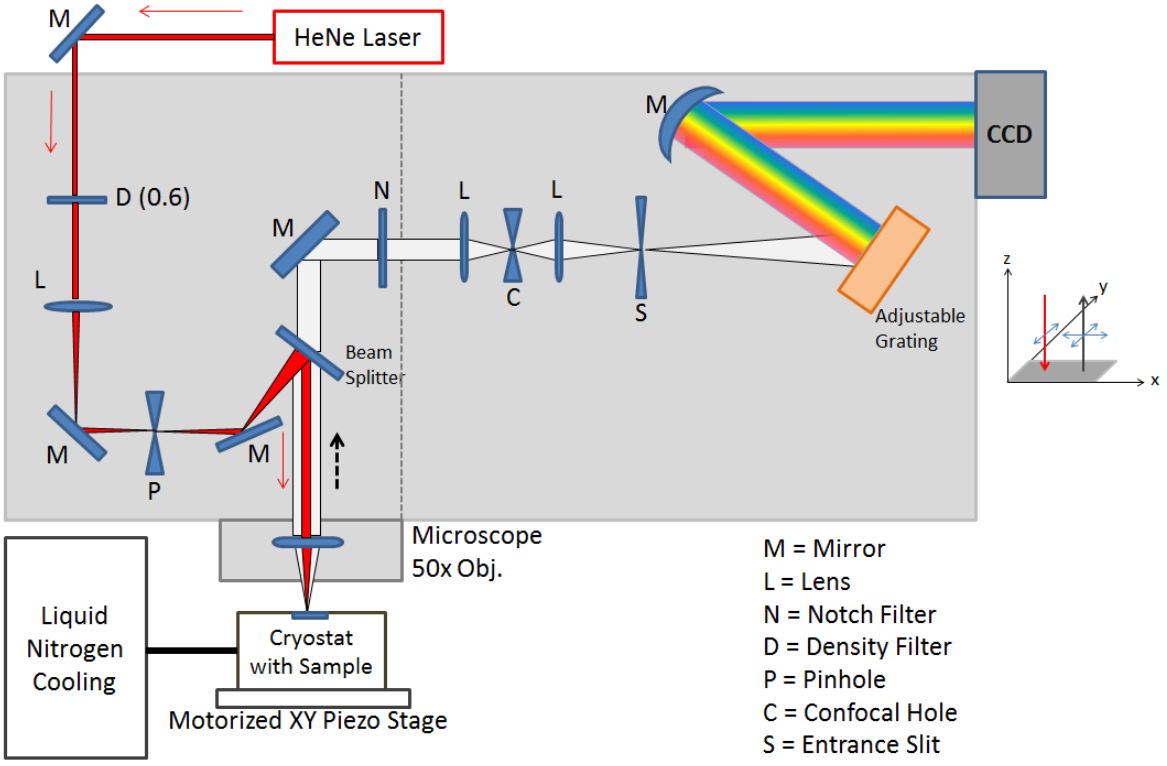

Figure 9: LabRam spectrometer HR800 with optical path of the laser beam, microscope, diffraction grating and CCD detector. The red beam represents the incident, the white one the polychromatic scattered beam. Right side: Scattering and polarization geometry of incident (red) and scattered (grey) light.

The laser beam is led through two irises, one in front of an interferential filter to eliminate plasma lines (for clarity, neither the irises nor the interferential filter are shown), and a density filter to regulate the power on the sample (D0.6 means a reduction by the factor $10^{-0.6} \approx \frac{1}{4}$), the other iris before the first lens, which focuses the beam on a spatial filter (pinhole size $1000\,\mu$m). This spatial filter is meant for point mode measurements; this so called confocal technique enhances resolution and minimizes undesired signal from lower excited sample volume by limiting the laser spot size on the sample. A notch filter which corresponds to the excitation laser line reflects the beam through a microscope with 50x magnification MSPlan objective with numerical aperture 0.55. The Raman fraction of the backscattered light follows the same path but passes the notch filter, while the Rayleigh fraction is blocked. The image is projected onto a confocal hole by a first lens, collected again and led to the spectrograph entrance slit by a second lens.

The spectrograph consists of a monochromator or diffraction grating and a CCD detector. The grating splits the incident polychromatic beam depending on the wavelength. Note that this grating has a preferential direction and is more sensitive to a polarization parallel to this direction. As there is no analyzer or lambda half plate implemented in this setup, no polarization direction is particularly selected, but horizontally polarized parts will lose a certain amount (the exact value is unknown) of intensity compared to the vertical ones. We measured with $600\,\frac{\mathrm{g}}{\mathrm{mm}}$ grating, the obtained spectrum covers roughly $100 - 1200\,\mathrm{cm}^{-1}$.

The actual detector is a CCD (Charge Coupled Device) array. The individual array elements - each responsible for a particular spectral position - are photo diodes (referred to as pixels). A CCD consists of a doped semiconductor covered by an insulating layer on which optically transparent electrodes are mounted. The incident light creates electron-hole pairs in the semiconductor which move seperately from each other with respect to the applied voltage. The resulting charge is then stored in the so called potential well; it is being processed as proportional signal to the incident luminous flux.

The sample is kept in an evacuated cryostat cooled by liquid nitrogen. The cryostat is mounted on a piezo controlled XY stage which allows fairly good control over the chosen focus spot. It is beneficial to excite, up to a certain degree of precision, the same spot for all spectra and temperatures to reach a maximum of comparability. This can be visually achieved by choosing a spot in between some markers or small dust particles on the sample surface by an applied camera, which at the same time allows to focus on the sample surface as exactly as possible.

The spectra are displayed and processed via the integrated Horiba software LabSpec. To avoid an excess of cosmic spikes in the spectra, a total of $70 \times 10\,\mathrm{s}$ spectra were taken and cumulated.

2.4 $LaVO_3$ and $La_{0.75}Sr_{0.25}VO_3$ Epitaxial Films: Fabrication and Structural Characterization

The epitaxial $LaVO_3$ and $La_{0.75}Sr_{0.25}VO_3$ films studied here were fabricated by Ionela Lindfors-Vrejoiu at the Research Center Jülich (PGI-7, in the labs of Prof. Regina Dittmann). The films were grown by PLD (Pulsed Laser Deposition) using a KrF excimer laser (248 nm, 20 ns laser pulses). The chamber was evacuated down to less than 10^{-7} mbar after the substrate was loaded into the PLD chamber. The substrates were heated to temperatures of about 450°C in high vacuum conditions. $Ar/4\%H_2$ gas mixture was let in the PLD chamber to pressures of $\approx 10^{-3}$ mbar and the substrates were further heated to 700°C and the films were grown under these ambient conditions. A laser energy density of $\approx 1.2\,\frac{\mathrm{J}}{\mathrm{cm}^2}$ was employed for the ablation of the ceramic targets and the laser repetition rate was 3 Hz. After growth the samples were cooled down to 300°C in the same Ar/H_2 atmosphere with a $20\,\frac{^\circ\mathrm{C}}{\mathrm{min}}$ cooling rate, and then the high power diode laser heater was switched off. In situ reflective high energy electron diffraction (RHEED) was used to monitor the growth mode and estimate the growth rate of the $LaVO_3$ films (see 12). The streaky RHEED pattern points to a satisfyingly even and good layer-by-layer growth.

Measurements on epitaxial films require certain considerations in comparison to single crystals. Due to the growth process and their low dimensions, they have to be grown on appropriate substrates. For the purpose of Raman spectroscopy, it is decisive to take the Raman activity of the substrate material into account, as potentially strong Raman active modes might hinder the observation of weak signals coming from the actual measured sample. A second important aspect to consider is the degree of lattice mismatch of substrate and film. Choosing the right substrates thus requires to balance out compatible lattice parameters on the one and a sufficiently undisturbing Raman activity on the other hand.

Gasparov *et al.* performed a systematic study of different single crystal with regard to their usability for Raman spectroscopy [4], the Raman characteristics are listed in the table (Fig. 10).

Table 1. Raman characteristics of the Raman references and substrates

Substrate	Dominant spectral features cm^{-1}	The main mode cm^{-1}	The main mode's m-number $10^{-8}\frac{cnts}{\frac{W}{m^2}s}$	I/I_{Si}	I/I_{CaF2}	Free spectral range (FSR) cm^{-1}	FSR background intensity I_{FSR}/I_{Si}	FSR background intensity I_{FSR}/I_{CaF2}	E_g eV
Si	520	520	45.5 ± 1.1	1.0	16	100–280 320–450 550–900	0.04	0.65	1.11[15]
CaF_2	321	321	2.8 ± 0.1	0.06	1.00	200–300 350–900	0.017	0.27	12[13]
TiO_2 rutile	234, 448, 612	612	59.9 ± 2.7	1.31	21.22	750–900	0.05	0.8	3[16]
$LaAlO_3$	32, 123	32	36.9 ± 4.5	0.81	13.1	180–475 510–900	0.01	0.19	5.6[17]
$SrTiO_3$	248, 305, 353, 621, 680, 716	305	21.2 ± 0.4	0.46	7.5	100–170 500–590	0.18 0.08	2.9 1.3	3.2[18]
$LaGaO_3$	59, 104, 120, 150	120	11.9 ± 0.3	0.26	4.23	480–900	0.01	0.16	4.4[19]
LSAT	467, 877	877	6.3 ± 0.2	0.14	2.3	170–400 660–830	0.013	0.21	>2.4
$NdGaO_3$	213, 448, 520, 732	213	5.1 ± 0.2	0.11	1.8	780–900	0.022	0.36	3.8[20]
$DyScO_3$	157, 308, 326, 355, 458, 474, 508	157	3.33 ± 0.06	0.07	1.2	570–900	0.011	0.18	5.9[21]
$YAlO_3$	148, 283, 343	282	3.27 ± 0.12	0.07	1.1	600–900	0.01	0.16	8.8[22]
$SrLaAlO_4$	323, 443, 665	443	1.13 ± 0.12	0.024	0.40	780–900	0.018	0.29	2.8[23]
MgO	No Raman modes, flat background		0.69 ± 0.06	0.015	0.24	100–900	0.015	0.24	7.8[24]

Figure 10: Table of the Raman characteristics of different materials. The free spectral range is particularly relevant as the present study mainly relies on the visibility of a certain phonon. The finally chosen substrates LSAT and $DyScO_3$ are marked by red boxes. [4]

Under consideration of various possible substrate materials, the finally used $LaVO_3$ film samples were grown on

- $(LaAlO_3)_{0.3}(Sr_2TaAlO_6)_{0.7}$ (LSAT)(100), cubic $Pm\bar{3}m$ with $a = 3.86$Å [12]
- $DyScO_3$ (DSO)(001), orthorhombic $Pbnm$ with $a = 5.442$Å, $b = 5.719$Å and $c = 7.904$Å [16]

Both substrates exhibit a free spectral range in the most important wavenumber range around $700\,cm^{-1}$ ($660 - 830\,cm^{-1}$ for LSAT and $570 - 900\,cm^{-1}$ for $DyScO_3$). The $La_{0.75}Sr_{0.25}VO_3$ thin film sample, used in order to study how A-site substitution (A-site refers to the designation ABO_3 with A=La, B=V) changes structural and physical properties, is grown on LSAT(100) as well.

For the purposes of Raman spectroscopy, the orientation of the out-of-plane axis of the $LaVO_3$ sample is an important aspect. Depending on the lattice of the substrate, the axis might grow in different orientations, as illustrated in Fig. 11.

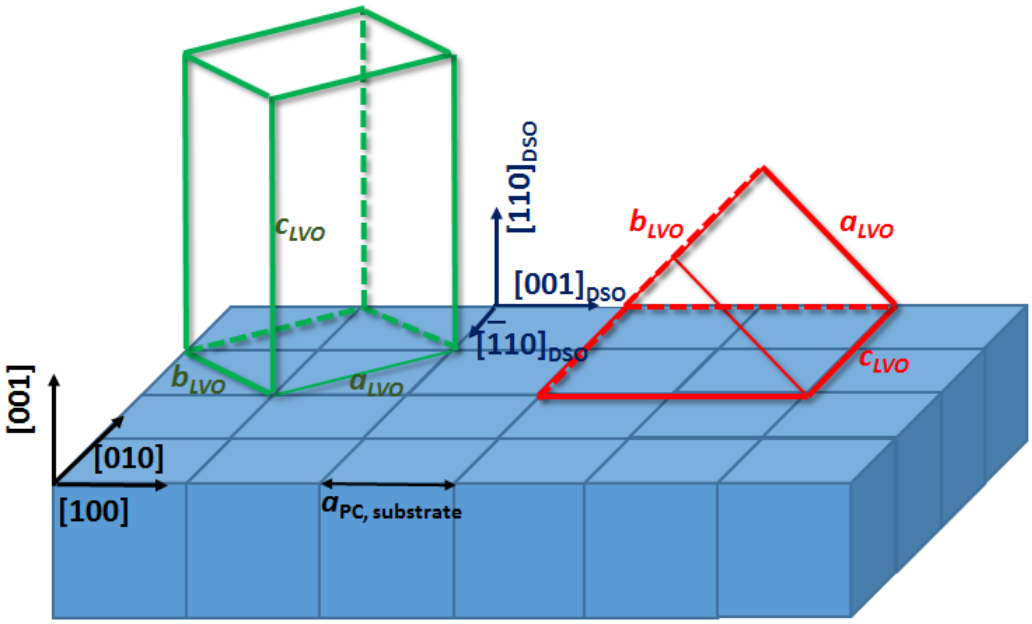

Figure 11: Schematics of matching the orthorhombic unit cell of $LaVO_3$ on a substrate with pseudocubic (PC) symmetry, such as LSAT(100) or $DyScO_3$/DSO(110), whose lattice parameters satisfy: $a_{PC} \approx \frac{a_{LVO}}{\sqrt{2}} \approx \frac{c_{LVO}}{2}$. Twin domains with the long orthorhombic c-axis in-plane (red) or out-of-plane (green) can form. Image by I. Lindfors-Vrejoiu.

The $DyScO_3$(001) substrate used in this study yields an important advantage in comparison with the $DyScO_3$(110) cubic or pseudocubic unit cell. In this orientation, the substrate only allows one type of growth with the long $LaVO_3$ orthorhombic c-axis perpendicular to the substrate surface. It should therefore be an excellent choice for Raman spectroscopy, as the internal structure of the film is relatively homogeneous, were it not for the fact that it exhibits very strong Raman active modes throughout a broad wavenumber range, see chapter 3.3.

As indicated in the sketch, when the sample is grown on LSAT, the film can grow in two possible orientation directions. Sclauzero *et al.* recently argued that there is neither of them is clearly preferred [17]; a more reliable statement can only be made by more detailed structural analysis. On the other hand, LSAT is an advantageous choice because it has only few Raman active modes. The spectral range relevant for the purpose of probing the phase transition to orbital order is basically free of distracting substrate signal.

To get a quantitative idea of the degree of lattice mismatch between sample and

substrate, the orthorhombic lattices (single crystal parameters of $LaVO_3$ are $a = 5.555$Å, $b = 5.553$Å and $c = 7.849$Å) can be projected on a pseudocubic structure (PC) according to a $a_{PC} \approx \frac{a}{\sqrt{2}} \approx \frac{b}{\sqrt{2}} \approx \frac{c}{2}$ relation [15].
LVO and LSVO in bulk have pseudocubic lattice constants [15] [19]

- $a_{PC,LVO}(bulk) = 3.925$Å
- $a_{PC,LSVO}(bulk) = 3.90$Å
- $a_{C,LSAT} = 3.86$Å $< a_{PC,LVO}$, compressive strain with a lattice mismatch $\Sigma_{LVO/LSAT} = -1.4\%$

The average lattice mismatch for the LSAT substrate was estimated as follows:

$$\Sigma = \frac{a_{Substrate} - a_{Film}}{a_{Substrate}}$$

In the case of $DyScO_3$, a_{DSO} is slightly smaller than a_{LVO} ($\Delta a \approx -0.11$), however, the mismatch of the b-axis is larger ($\Delta b \approx +0.16$), hence, in average, the unit cell is exposed to tensile strain.

This mismatch and therefore the compressive or tensile strain potentially affects thin film properties. Under preservation of the overall unit cell volume, the strain tends to lead to a change in lattice parameters. This has been reported for different materials to result in a slight shift of optical mode frequencies, namely to lower wavenumbers in the case of tensile strain (e.g. for GaAs epitaxial layers, cf. [13]) and to higher wavenumbers when compressive strain is imposed (e.g. for the proton conductor $BaCe_{0.8}Y_{0.2}O_{3-\delta}$, cf. [2]).

Compressive strain on one hand causes the out-of-plane-axis to elongate while the atoms in the ab-plane are forced closer together, the opposite holds for the case of tensile strain. The adjustment of the film lattice structure due to epitaxial strain can be visualized and quantitavely determined by X-ray diffraction analysis of LVO/LSVO in comparison to the cubic LSAT substrate. Fig. 12 b) indicates an elongation of the out-of-plane lattice parameter, visualized by a shift of the respective Bragg peak angles to the left hand side with respect to the cubic (100) and (200) reflections of LSAT.

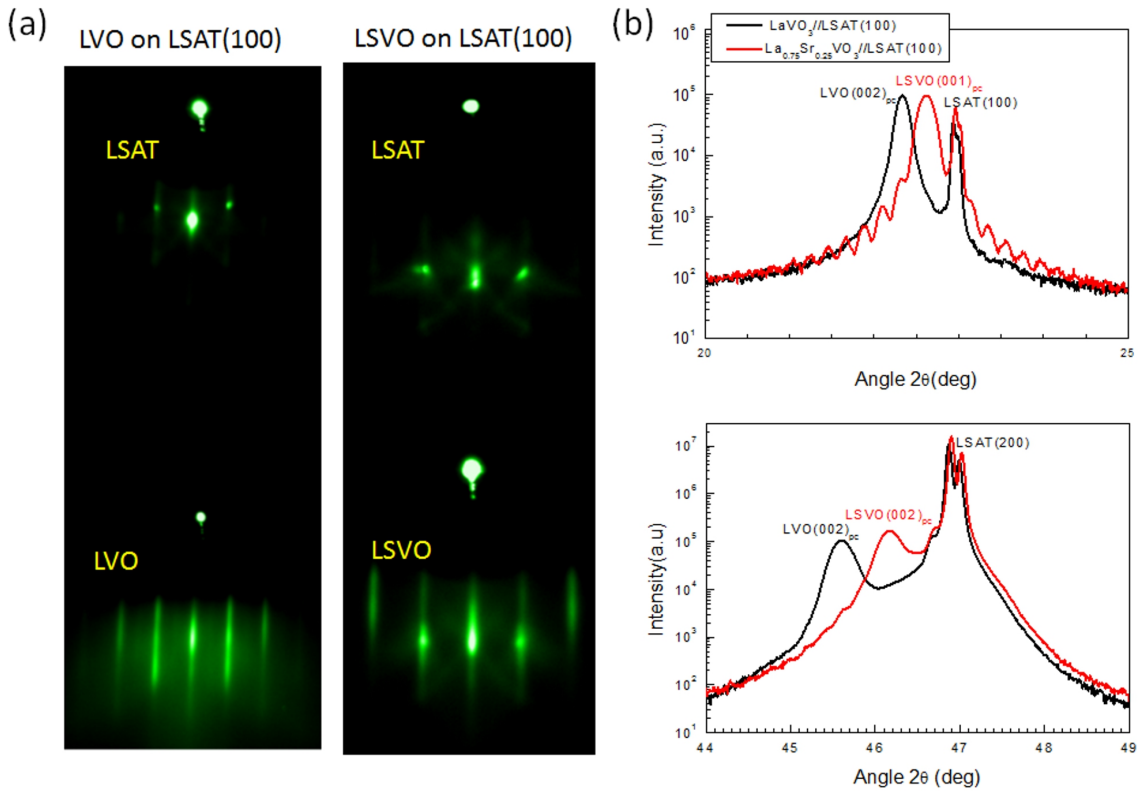

Figure 12: (a) RHEED patterns of the LSAT substrates just prior to film growth and of the $LaVO_3$ (LVO) or $La_{0.75}Sr_{0.25}VO_3$ (LSVO) films just after the growth, indicating layer-by-layer epitaxial growth. (b) $\Theta - 2\Theta$ XRD scans around the (100) and (200) LSAT reflections for the $LaVO_3$ and $La_{0.75}Sr_{0.25}VO_3$ films. The LVO film has larger out-of-plane lattice parameter than the LSVO film. RHEED and XRD data are provided by I. Lindfors-Vrejoiu.

The streaky RHEED pattern of the LVO and LSVO film shown in Fig. 12 indicates layer-by-layer growth.
Analysis of the X-ray diffraction of LVO/LSVO and LSAT allows to calculate the increased thin film lattice constants:

- $a_{PC,LVO} = 3.97$Å
- $a_{PC,LSVO} = 3.927$Å

Structural adjustment of the lattice constants on the one and the mixture of orientation domains on the other hand might affect the quality of the obtained Raman spectra in comparison to measurements on high quality single crystals, as a clean and homogeneous sample facilitates the interpretation of the observed features.

3 Temperature-dependent Raman Spectroscopy of Orbital-Ordered Lanthanum Vanadate Films: Experimental Data and Interpretation

The results of the temperature-dependent Raman measurement sequences carried out in Freiberg are presented and discussed in the following section.

3.1 $LaVO_3$ on LSAT(100)

The first measurement sequence was carried out on $LaVO_3$ on a (100)-oriented LSAT substrate from 90 K up to room temperature (296 K) in order to study the temperature dependence of the Raman active modes in $LaVO_3$. For each temperature, the laser beam was first focused on the sample surface to catch as much signal of the 70 nm thin film as possible, followed by a second measurement 30 μm below the surface to obtain the spectrum of the underlying LSAT substrate.

Fig. 13 shows spectra of four different temperatures around the presumed transition temperature. To allow a direct comparison, the solid lines represent the surface measurements while the dotted lines show those taken in the substrate. The arrows point to the possible $LaVO_3$ film contributions. Towards room temperature, the peaks are slightly broadened.

Although a slight elevation around 700 cm^{-1} is already observable at room temperature, it is visibly enhanced below 150 K.

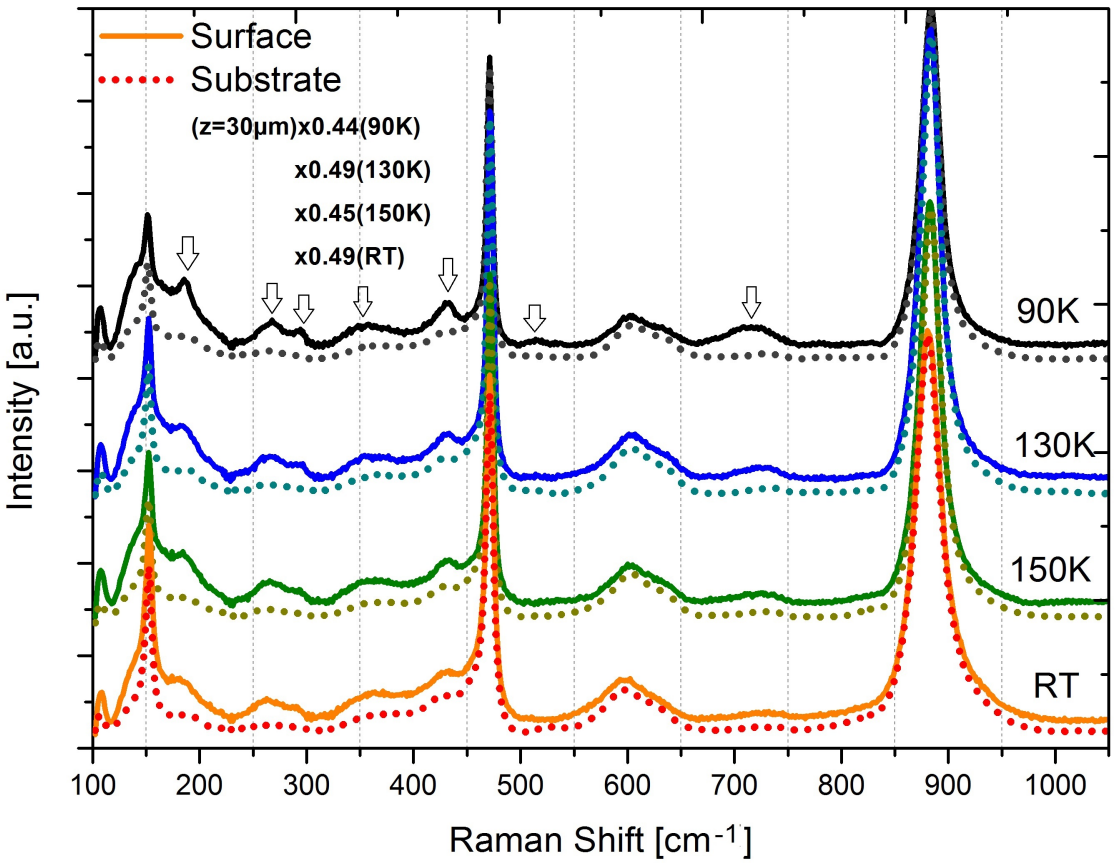

Figure 13: Raman spectra above and below the phase transition temperature. The solid lines show the signal on the sample surface while the dotted spectra have been taken 30 μm below the surface. The latter have been normalized to the respective intensity (z= 30 μm×normalization factor). The black arrows indicate the modes corresponding to the $LaVO_3$ film.

The original signal intensity of the substrate was significantly higher when the laser was focused deeply into the sample in camparison to the surface measurement. For further processing, the spectra were normalized to the same intensity by a factor given in the graph (z= 30 μm×normalization factor).

We find four major contributions of the substrate at 151 cm^{-1}, 471 cm^{-1}, 884 cm^{-1} and in the range of 575 − 650 cm^{-1}. These features do not hinder the recognition of most of the expected signals of $LaVO_3$. Under this aspect, LSAT has been a suitable choice as substrate, as it allows to observe the $LaVO_3$ Raman features in reasonably undisturbed quality. The subtraction of the normalized substrate spectrum allows to extract the actual $LaVO_3$ spectrum, see Fig. 14.

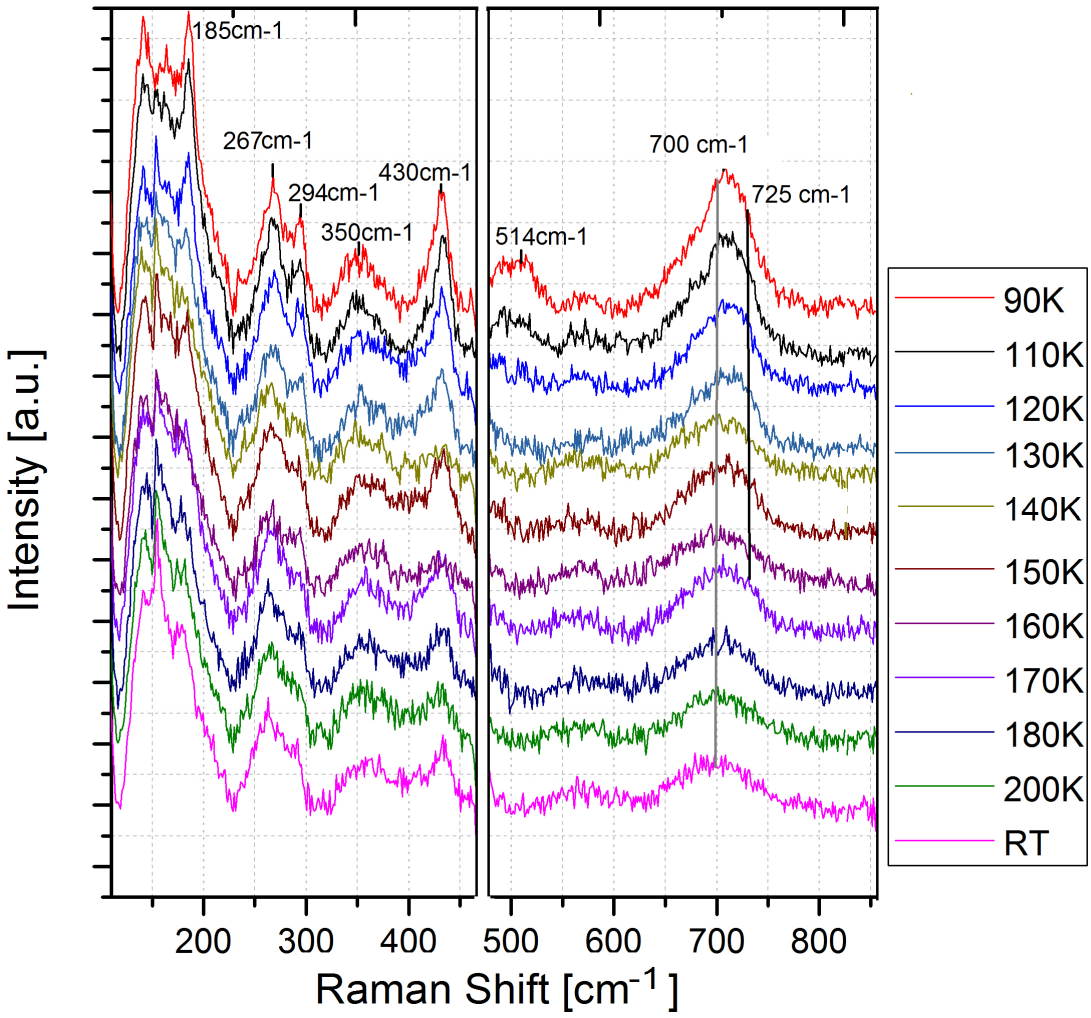

Figure 14: $LaVO_3$ spectrum after substrate subtraction. Particularly in the low energy range, the peak quality partially suffers from the subtraction of close underlying LSAT modes: the A_g phonon at $487\,cm^{-1}$ is covered completely by a major LSAT mode. The vertical lines indicate the room temperature peak center at $700\,cm^{-1}$ and, for comparison, the increasingly shifted centroid towards about $725\,cm^{-1}$ due to the additional phonon.

The subtracted spectra show all expected features, except from the A_g phonon at $487\,cm^{-1}$ (see Fig. 14). The spectrum in the vicinity of the $185\,cm^{-1}$ phonon does not exclusively result from $LaVO_3$. This range is suffering from a strong upperlying substrate contribution in the $100 - 200\,cm^{-1}$ wavenumber range.

Comparing with the data on single crystals (cf. 1), the peaks at 185, 430 and $514cm^{-1}$ have experienced a slight shift to higher wavenumbers (they correspond to the following values: 182, 428 and $511cm^{-1}$. The opposite holds for the peaks at 267 and $294\,cm^{-1}$ (which are located at 271 and $297\,cm^{-1}$ in the bulk spectrum, respectively). The shift

might result from the compressive strain imposed by the substrate, however, exact quantitative statements are rather not possible given the quality of the data. Moreover, as this sample is most likely very unevenly grown, the strain does probably not have one distinct effect in terms of an overall observable trend.

As phonon modes are generally softened at higher temperatures due to thermal broadening, the peaks get sharper and the intensity is increased towards 90 K. The temperature dependent presentation allows to compare the development of the different modes with decreasing temperature. This dependency indicates whether the respective modes are correlated with the structural phase transition and the onset of orbital ordering.

While the intensity of the phonons at $185\,\mathrm{cm}^{-1}$, $267\,\mathrm{cm}^{-1}$ and $294\,\mathrm{cm}^{-1}$ is nearly preserved up to room temperature, the intensity of the peaks at $430\,\mathrm{cm}^{-1}$ and $700 - 725\,\mathrm{cm}^{-1}$ is gradually decreased. The data do not really allow to make any statement concerning the temperature dependence of the potential orbital excitations which are supposed to be located around $350\,\mathrm{cm}^{-1}$ and $514\,\mathrm{cm}^{-1}$ according to Miyasaka *et al.*, see chapter 2.2. The $350\,\mathrm{cm}^{-1}$ peak seems to get enhanced at lower temperatures, but a clear trend is not observable. The main contribution might actually come from the substrate, hence the extraction of the potential two-orbiton peak of $LaVO_3$ is hardly possible. Comparing with the $LaVO_3$ spectrum of Miyasaka *et al*, we see that this peak is very weak even in single crystal measurements (cf. chapter 2.2).

On the other hand, the $514\,\mathrm{cm}^{-1}$ peak is probably affected by the vicinity of the strong $471\,\mathrm{cm}^{-1}$ substrate mode. It is only visible at 110 and 90 K. In this respect, the present data are insufficient in terms of a meaningful analysis.

According to comparable measurements by Vrejoiu *et al.* [19] and Roberge *et al.* [14], the peak at $700 - 725\,\mathrm{cm}^{-1}$ is actually a double peak consisting of the phonon density of states around $700\,\mathrm{cm}^{-1}$, already visible as a broad elevation at room temperature, and another one in close vicinity at around $720\,\mathrm{cm}^{-1}$ which is supposed to appear below T_{OO}.

The PDS peak and the peak assigned to the $B1_g(1)$ mode of the OO phase are not resolved down to the lowest temperature at which measurements could be performed. However, it becomes increasingly asymmetric with decreasing temperature. This asymmetry is observable for the first time around 170 K, however, as the 160 K spectrum looks rather symmetrical again, a more exact determination of the transition temperature in the epitaxial film is very difficult. At lower temperatures, the centroid is clearly shifted

towards 725cm^{-1}. The asymmetric shape and the growth indicate the occurrence of the second peak below the transition temperature.[2]

This is shown more clearly by a direct comparison of the peak at 700cm^{-1} at room temperature and below, as shown in Fig. 15.

[2]The spectra recorded at 160 K and 140 K do not really match this general trend but are of a rather bad quality in comparison. The asymmetric peak shape around 725cm^{-1} is not observable in these cases. They might suffer from imprecise focusing.

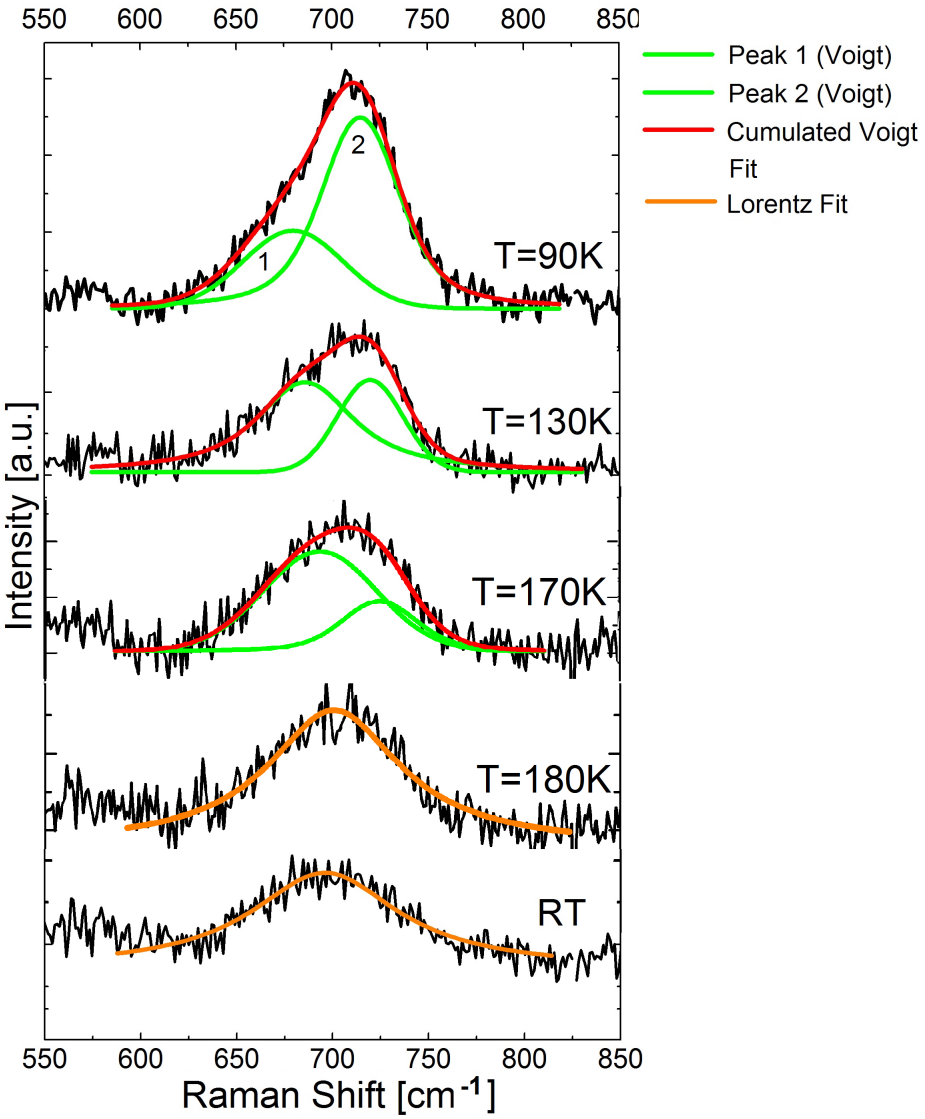

Figure 15: The peak around 700 cm^{-1} for different temperatures. While the peak shape corresponds to a single Lorentz function at RT and 180 K (orange curves)), the slightly deviating shape can be reproduced by the cumulation of two Voigtian peaks at lower temperatures (green and red curves, respectively). The green peaks 1 and 2 are marked as such (see the T= 90 K plot).

While the peak can be described quite good by a single Lorentz function at room temperature and still at temperatures as low as 180 K, the peak is described better by a cumulation of two Voigtian peaks at lower temperatures. This provides support to the presumption of the appearance of a second peak at $T_{OO} \approx 170$ K (green curve at the right hand side), which is growing with decreasing temperature.

The possibility to resolve the double peak at $700 - 725$ cm^{-1} might be inhibited by the high degree of strain and the thereby induced structural modifications. The average change of the unit cell lattice parameters in the film appears to broaden the phonon mode to a relatively high extent, moreover, it is not possible to separate the contributions of domains with differently oriented orthorhombic c-axis (see chapter 2.4). Limiting factors might also arise from the setup itself: On one hand, the energy resolution could be too low. However, as the wavenumber difference between the two peaks should be approximately $20\,\mathrm{cm}^{-1}$, the structural inhomogeneities probably play a more decisive role, as can be seen by the comparison of the fairly distinct peaks at $267\,\mathrm{cm}^{-1}$ and $294\,\mathrm{cm}^{-1}$ with $\Delta\overline{\nu} = 26\,\mathrm{cm}^{-1}$. Another possibility might be the fact that the measurements have been performed with unpolarized scattered light detection and without any waveplate. The unequal sensitivity of the spectrometer to differently polarized light might result in a loss of accuracy and separation capability. However, in a comparable spectrum of $LaVO_3$ grown on twinned $LaGaO_3((110)/(001))$, which has been acquired by the same setup in Freiberg by Vrejoiu *et al.*, the double peak structure is somewhat better resolved (cf. [19]). Hence, the broad peak shape is probably rather due to the structural inhomogeneity of the $LaVO_3$ film on LSAT, due to the larger compressive strain.

At the same time, this structural inhomogeneity of the film could be the reason why the spectrum shows signal around $700\,\mathrm{cm}^{-1}$, assigned to the phonon density of states at room temperature, at the first place. In the data of Miyasaka *et al.* (see chapter 2.2), no such feature is recognizable, or at least it shows significantly lower intensity, whereas it is visible not only in the present data but also in the aforementioned studies on $LaVO_3$ single crystals by Roberge *et al.* (cf. [14]) and on thin films grown on twinned $LaGaO_3(110/001)$ and $DyScO_3(110)$ (cf. [19]). This is probably due to the fact that the single crystal sample used by Miyasaka *et al.* has been of better quality in terms of composition and non-twinned structure, but it is not entirely clear under which specific conditions the phonon density of states at $700\,\mathrm{cm}^{-1}$ does appear or not. Yet, this underlying peak complicates a quantitative analysis of the phonon correlated to the orbital-ordered phase, as we can only assume how one or the other mode behaves with decreasing temperature.

As the asymmetric peak shape seems to appear already around 170 K, the transition into an orbital-ordered state seems to be shifted to higher temperatures with respect to the OO transition temperature for $LaVO_3$ single crystals. However, this phenomenon is not unknown in epitaxial films. It might result from internal structural modifications or inhomogeneities due to the epitaxy induced strain as well [19].

3.2 $La_{0.75}Sr_{0.25}VO_3$ on LSAT(100)

The second measured sample was a $La_{0.75}Sr_{0.25}VO_3$ epitaxial film grown on LSAT(100). The spectra were processed as described in the former chapter. The direct comparison of dotted and solid lines (which belong to the deeper focused substrate and surface signal, respectively) immediately shows a significantly reduced signal obtained from the Sr-substituted compound.

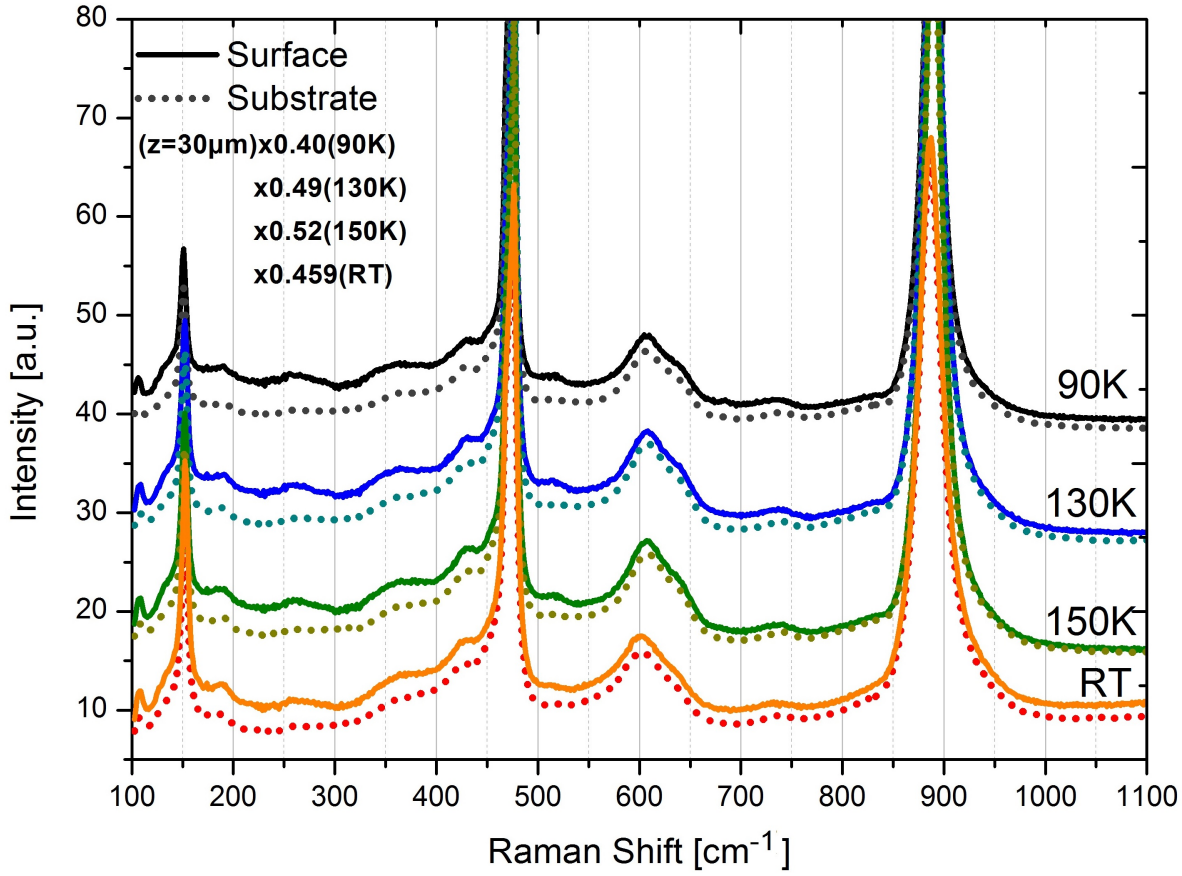

Figure 16: Raman spectra for different temperatures of a $La_{0.75}Sr_{0.25}VO_3$ film grown on LSAT(100). The dotted lines correspond to the substrate, the solid spectrum has been recorded focusing on the film.

The subtraction of the normalized spectra shown in Fig. 17 reveals that the signal has almost completely disappeared. Only residues of very low intensiy are visible. Obviously, the G-type orbital-ordered phase is strongly affected by Sr substitution.

However, this does not necessarily mean that orbital order is destroyed in general. If orbital order occurs in LSVO, the transition temperature is probably much lower than

90 K. This goes along with prior investigations on LSVO single crystals and Raman measurements on $Nd_{1-x}Sr_xVO_3$, cf. chapter 1.2.1.

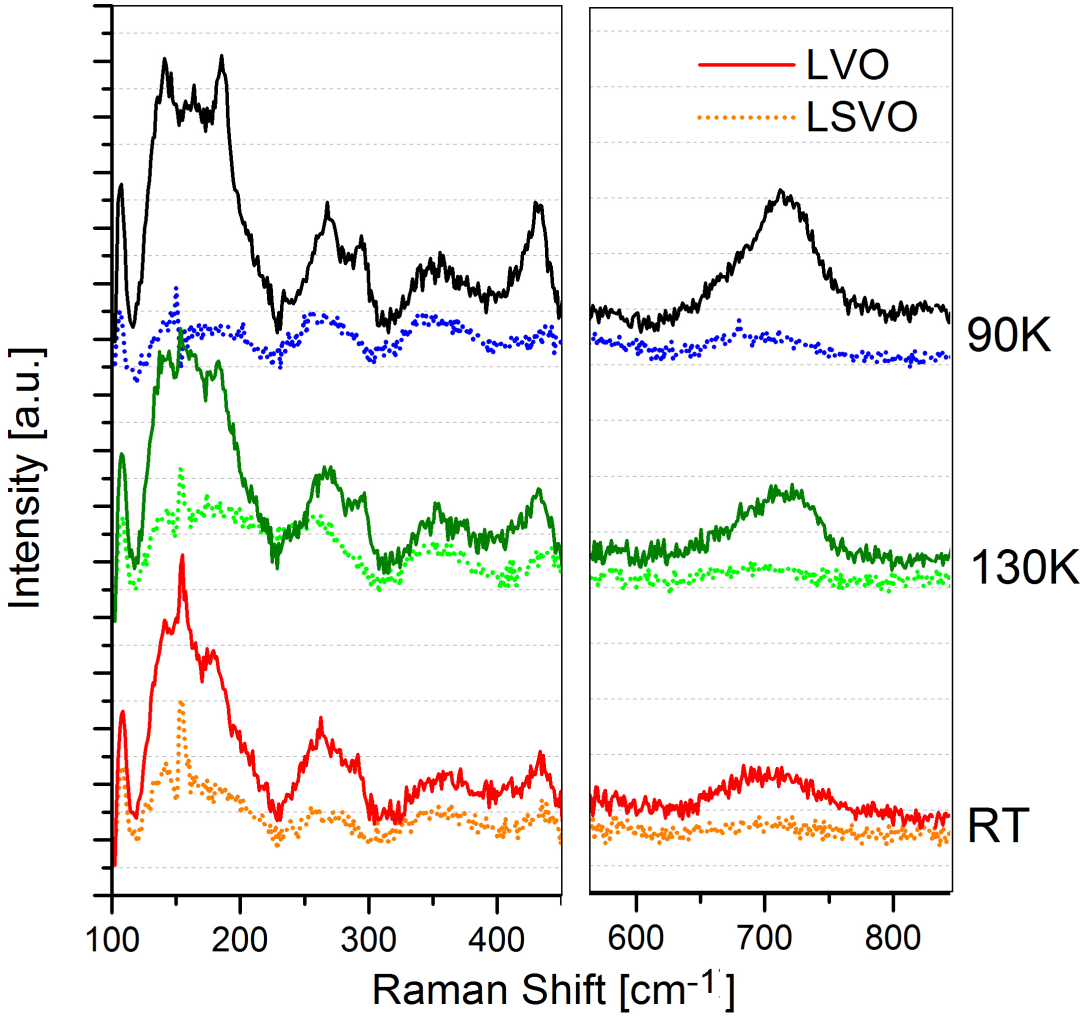

Figure 17: Temperature-dependent spectra of the pure $LaVO_3$ film (solid, LVO) in comparison to the $La_{0.75}Sr_{0.25}VO_3$ (dotted, LSVO). The Raman signal of LSVO is considerably lower.

The signal residues might indicate that the structural phase transition into a "Raman forbidden" cubic O_h point group is not concluded throughout the whole film. Yet, the intensity does not visibly change from RT to 90 K; particularly the peak around 700 cm^{-1} which is significantly enhanced below 170 K due to the onset of OO does not change in any way with decreasing temperature. The phonon polarizability and intensity, respectively, is therefore not changed in the given temperature range. Further information concerning the structural change in Sr-substituted $LaVO_3$ could only be provided by measurements at much lower temperatures.

3.3 $LaVO_3$ on $DyScO_3(001)$

The third measured sample was a $LaVO_3$ film grown on a $DyScO_3$ substrate, which imposes tensile strain due larger lattice constants. Almost all $LaVO_3$ modes are hidden by the strong Raman active modes of $DyScO_3(001)$ in the wavenumber range from 100 to 550 cm^{-1}, only the phonons at 178 cm^{-1} and around 294 cm^{-1} can be recognized. This makes the substrate a slightly problematic choice for Raman spectroscopy, as the informational content is strongly limited.

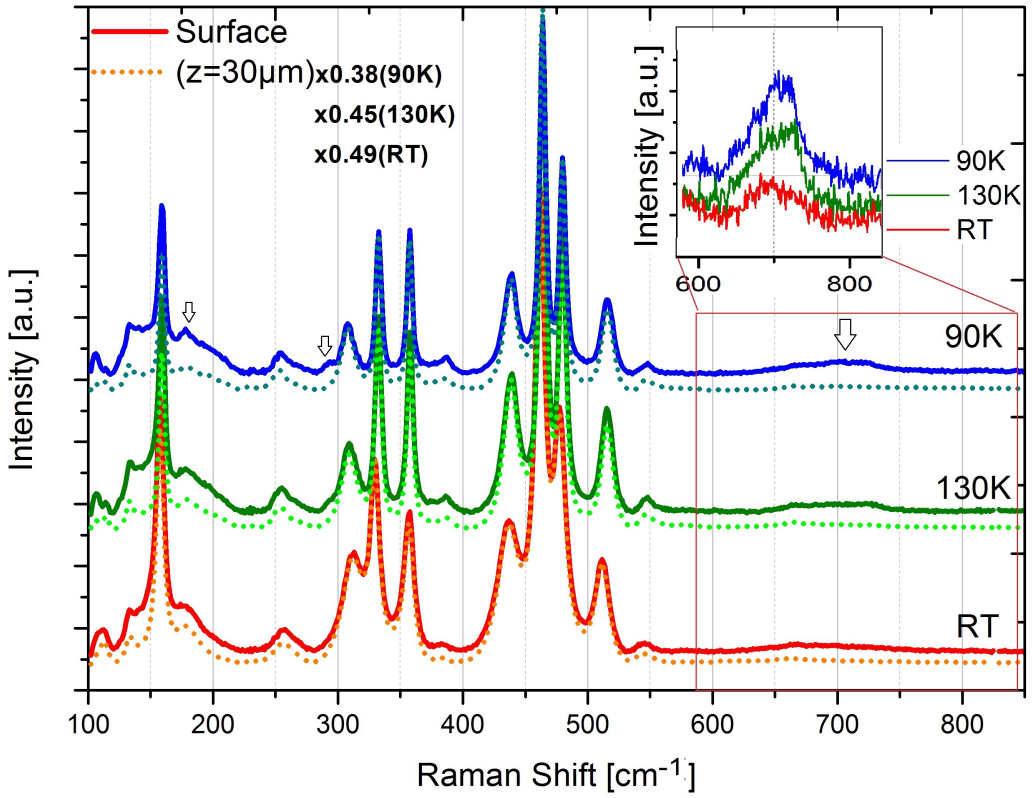

Figure 18: Temperature-dependent Raman spectra of a $LaVO_3$ film grown on $DyScO_3(001)$. The black arrows indicate the contributions from the film. The inset shows the extracted $LaVO_3$ spectrum after normalization by the given factor and subsequent subtraction in the wavenumber range $600 - 800\,cm^{-1}$.

All peaks seem to be slightly shifted towards lower energies in comparison to the sample grown on LSAT. This shift goes well with the tendencies indicated in prior publications on other materials (cf. chapter 2.4); the strain effect in this particular sample on DSO(001) might furthermore be more homogeneous distributed than in the former sample grown on LSAT, as the film structure should be less twinned. It is expected in this case that the c-axis of the $LaVO_3$ film is mainly perpendicular to

the DSO(001) substrate surface. The peaks at 178 cm^{-1} and around 294 cm^{-1} are in the case of LSAT located at 182 cm^{-1} and 297 cm^{-1}, respectively. The same applies to the phonon density of states peak; the peak maximum is located at 700 cm^{-1} in single crystal measurements as well as in the LSAT sample. The inset of the plot presents a subtracted spectrum which was obtained by the same procedure as described in chapter 3.1: the respective peak appears substantially sharper after substraction and allows to monitor the development with decreasing temperature. In agreement with the general trend, the peak maximum at room temperature is around 690 cm^{-1}. At 130 K, it shows a significant asymmetry which indicates the appearance of a second mode with the maximum at 723 cm^{-1}. The asymmetry is reduced again at 90 K, nevertheless, the peak maximum is still located close to 723 cm^{-1}. A direct comparison to the former measurement sequence of $LaVO_3$ on LSAT is of course possible only to a limited extent, as the corresponding temperature dependent series from 90 K to room temperature is not available in this case. Moreover, most peaks are completely covered by the strongly obstructive substrate signal. Yet, a small trend of a shift towards lower photon energies is recognizable, although this estimation is rather uncertain due to a high noise level. This possibly corresponds to the fact that the average out-of-plane lattice parameters are slightly shortened for the $LaVO_3$ film grown on DSO(001) compared with the film grown on LSAT(100). The possibility to resolve this double-peak at temperatures as low as 90K seems to be impeded in a similar way with respect to $LaVO_3$ on LSAT, which can probably be ascribed to a structurally inhomogeneous crystal (due to strain relaxation along the growth direction), even although this problem should be reduced in the sample grown on $DyScO_3$(001), as the film should grow more uniformly in terms of orientation (see chapter 2.4).

3.4 Summary: Evaluation of the Experimental Results and Conclusion

The investigations carried out in the scope of this thesis aimed on demonstrating that orbital ordering is present in $LaVO_3$ epitaxial films under both compressive and tensile strain imposed by the respective substrate and, on the other hand, can be destroyed by A-site Sr-substitution in $La_{0.75}Sr_{0.25}VO_3$.

Prior investigations of single crystals showed that $LaVO_3$ undergoes a structural phase transition accompanied by the onset of orbital order. Proving experimental evidence for this transition to happen in thin epitaxial films as well turned out to be slightly difficult in some respects: both resistivity measurements and SQUID magnetometry could not provide valuable results. In the case of the transport measurements, the resistivity of the sample strongly increased up to values that could not be processed any more by the setup towards lower temperatures; moreover, the conduction properties of the $LaVO_3$ thin films turned out to strongly depend on the chosen substrate, as the aforementioned insulating behaviour was observed in a sample grown on $DyScO_3(110)$, whereas it behaved like a metal when grown on $SrTiO_3(100)$ (cf. [19]). For the purpose of SQUID magnetometry, the magnetic response of the film was dominated by the substrate and not extractable.

However, Raman spectroscopy is a suitable technique to probe structural transitions, as it yields information concerning the specific lattice oscillations depending on their symmetry and is therefore highly sensitive to structural changes. The structural phase transition and thus the onset of orbital order has its fingerprint in a $LaVO_3$ Raman spectrum, particularly in the occurrence of a phonon around $720\,cm^{-1}$ below the transition temperature. Furthermore, the Raman spectrum of $LaVO_3$ is discussed to allow the observation of collective orbital excitations (two-orbitons) at 350 and $511\,cm^{-1}$.

To verify if the orbital-ordered state is present in epitaxial films as well, we first recorded temperature-dependent Raman spectra from room temperature down to 90 K of $LaVO_3$ grown on LSAT(100). This material has been chosen as substrate for the fact that it exhibits rather few Raman active modes and therefore has large free spectral range which allows to observe most of the features coming from the $LaVO_3$ film. As it has somewhat smaller lattice parameters, LSAT imposes a rather high degree of compressive

strain (about -1.4% at RT) on the film, which results in both slightly enlargened out-of-plane axis parameters and the development of domains in which the out-of-plane axis is oriented in different directions.

The second sample was a $La_{0.75}Sr_{0.25}VO_3$ epitaxial film, grown on LSAT as well. The comparison to the pure $LaVO_3$ sample allows to examine the structural change in to a Raman-inactive crystal point group due to the Sr-substitution, as indicated by single crystal data of comparable materials.

Finally, a comparative study was performed on $LaVO_3$ films grown on $DyScO_3(001)$, which imposes tensile strain due to the slightly larger lattice parameters. $DyScO_3$ has strong Raman active modes but allows to observe the peak of the $LaVO_3$ film around $720\,cm^{-1}$ as well, which is crucial as its occurrence correlated to the structural phase transition accompanied by the onset of orbital order. It should furthermore allow the film to grow in only one orientation with the c-axis perpendicular to the substrate surface and therefore produce a somewhat cleaner sample in terms of structural domain orientation.

The results show that orbital order is present in the $LaVO_3$ films in a comparable way as in single crystals. Detailed and unambiguous analysis of the respective peaks is difficult, probably due to inherently inhomogeneous structure of epitaxial film samples which are affected by the substrate-induced compressive or tensile strain. General strain-related tendencies in terms of shifts of phonon frequencies are partially observable, but the data quality limits a detailed evaluation. Raman measurements of thin films on substrates are inherently complicated with respect to spectroscopy on single crystals, as the actual desired film signal has to be extracted from the collective spectrum by subtraction. This procedure potentially affects the realistic sample spectrum in terms of peak shape and intensity.

In case of the $La_{0.75}Sr_{0.25}VO_3$ films, it could be shown that long-range orbital order is not persistent any more at this Sr concentration level and at temperatures as low as 90K. The crystal structure of the substituted compound has probably changed to a Raman inactive point group, presumably into cubic symmetry. A potential structural phase transition does at least not take place within the temperature range from room temperature to 90 K, but might happen at lower temperatures. Small signal residues might nonetheless indicate that the structure has not changed homogeneously throughout the whole film.

In conclusion, the measurements provide evidence for the existence of an orbital-ordered phase in pure $LaVO_3$ epitaxial films grown on different substrates. Compared with Raman scattering spectra of bulk $LaVO_3$ single crystals, the thin film samples on LSAT substrates exhibited all the Raman bands observed for the bulk as well, except from one peak which was dominated by a strong substrate mode. Further clarification concerning the observed peaks at $350\,cm^{-1}$ and $514\,cm^{-1}$ and their respective origin can not be provided by the present spectra, as a detailed analysis of the presumed collective orbital excitations (so called two-orbitons) is not possible due to a insufficient data quality.

Further indications of their actual origin requires better data and thus measurements on very clean and uniformly grown single crystals. Furthermore, Raman spectroscopy alone cannot elucidate the origin of these excitations; additional experiments following different or complementary approaches, like, for example, Raman spectroscopy in an applied magnetic field and resonant inelastic X-ray scattering, will be needed to gain deeper understanding of the material properties. Concomitantly, it may also be beneficial to measure in temperature ranges below 90 K, as the quality of the acquired data usually enhances in terms of signal-to-noise ratio and peak sharpness. This applies particularly to the Sr-substituted compound, as a potential phase transition probably takes place at much lower temperatures.

Appendix

Lorentzian and Voigt Fit Data

Lorentz fits for room temperature and 180 K. Fit function:

$$y = y_0 + \frac{2A}{\pi}\left(\frac{w}{4(x-x_c)^2 + w^2}\right)$$

Assignment of Lorentz parameters: y_0 =Offset, x_c =Center, A =Area, w =Width

Table 2: Lorentz Fit Parameters for Room Temperature and 180 K

RT		
Parameter	Value	Standard Error
y0	-0.2137	3.2530E-2
xc	695.9398	1.0596
w	93.1711	6.9052
A	125.8144	12.1240
H	0.8597	
180 K		
y0	-0.1095	3.022E-2
xc	700.6009	0.9944
w	83.8222	5.7658
A	127.7444	10.7348
H	0.9702	

Voigt fits for 170, 130 and 90 K. Fit function:

$$y = y_0 + A\frac{2\ln 2}{\pi^{\frac{2}{3}}}\frac{W_L}{W_G^2}\int_{-\infty}^{+\infty}\frac{e^{-t^2}}{\left(\sqrt{\ln 2}\frac{W_L}{W_G}\right)^2 + \left(\sqrt{4\ln 2}\frac{x-x_c}{W_G} - t\right)^2}dt$$

Convolution formula:

$$y = y_0 + (f_1 * f_2)(x)$$

with

$$f_1 = \frac{2A}{\pi}\frac{w_L}{4(x-x_c)^2 + w_L^2}$$

and

$$f_2 = \sqrt{\frac{4\ln 2}{\pi}}\frac{e^{\frac{4\ln 2}{W_G^2}*x^2}}{w_G}$$

Assignment of Voigt parameters: y_0 =Offset, x_c =Center, A =Area, w_G =Gaussian FWHM, w_L =Lorentzian FWHM

Table 3: Voigt Fit Parameters for 170, 130 and 90 K

170 K		
Parameter	Value	Error
y0	1.3860E-2	2.5000E-2
xc1	693.629	19.3326
A1	60.2482	43.2327
wG1	70.2522	16.8807
wL1	3.2464E-17	–
xc2	724.7772	5.5735
A2	23.0690	45.8738
wG2	37.6330	31.2947
wL2	15.7004	28.1162
130 K		
y0	2.7210E-2	3.3200E-2
xc1	685.9506	9.9902
A1	74.1551	26.8842
wG1	21.1311	29.2504
wL1	52.9889	18.0130
xc2	719.9242	4.2417
A2	35.7226	17.5856
wG2	40.2777	8.5012
wL2	3.2318E-17	–
90 K		
y0	3.5700E-3	2.5920E-2
xc1	679.8412	11.5454
A1	49.8730	23.1630
wG1	61.6356	11.6624
wL1	3.8853E-14	0.8617
xc2	714.8895	1.9524
A2	117.7220	21.8058
wG2	34.1001	8.0511
wL2	23.8450	8.7072

Table 4: Voigt Fit: Gaussian and Lorentzian Widths for 170, 130 and 90 K

170 K	Area	Center	Gaussian Width	Lorentzian Width
1	60.2482	693.6292	70.2521	3.2464E-17
2	23.0690	724.7772	37.6330	15.7004
130 K				
1	74.1551	685.9506	21.1311	52.9889
2	35.7226	719.9242	40.2777	3.2318E-17
90 K				
1	49.8730	679.8412	61.6356	3.8853E-14
2	117.7220	714.8895	34.1001	23.8450

References

[1] P. Bordet, C. Chaillout, M. Marezio, Q. Huang, A. Santoro, S.-W. Cheong, H. Takagi, C.S. Oglesby, and B. Batlogg: Structural aspects of the crystallographic-magnetic transition $LaVO_3$ around 140 K. In: *J. Solid State Chem.* **106**, 253-270(1993).

[2] Q. Chen, T.-W. Huang, M. Baldini, A. Hushur, V. Pomjakushin, S. Clark, W.L. Mao, M.H. Manghnani, A. Braun, and T. Graule: Effect of compressive strain on the Raman modes of the dry and hydrated $BaCe_{0.8}Y_{0.2}O_3$ proton conductor. In: *J. Phys. Chem. C* **2011** *115*(48), pp 24021-24027.

[3] J. Fujioka, S. Miyasaka, and Y. Tokura: Orbital disordering and the metal-insulator transition with hole doping in perovskite-type vanadium oxides. In: *Phys. Rev. B* **72**, 024460 (2005).

[4] L. Gasparov, T. Jegorel, L. Loetgering, S. Middey, and J. Chakhalian: Thin film substrates from the Raman spectroscopy point of view. In: *J. Raman Spectrosc.* **45**, 465-469 (2014).

[5] M. Grüninger, R. Rückamp, M. Windt, P. Reutler, C. Zobel, T. Lorenz, and A. Freimuth: Experimental quest for orbital waves. In: *Nature* **418**, 39 (2002).

[6] P. Horsch: Orbital physics in transition metal oxides: Magnetism and optics. In: *Handbook of Magnetism and Advanced Magnetic Materials (Fundamentals and Theory)*, ed. H. Kronmüller and S. Parkin, New York: Wiley (2007).

[7] M. Iliev, M.V. Abrashev, H.-G. Lee, V.N. Popov, Y.Y. Sun, C. Thomsen, R.L. Meng, and C.W. Chu: Raman spectroscopy of orthorhombic perovskitelike $YMnO_3$ and $LaMnO_3$. In: *Phys. Rev. B* **57** 2872(1998).

[8] F. Inaba, T. Arima, T. Ishikawa, T. Katsufuji, and Y. Tokura: Change of electronic properties on the doping-induced insulator-metal transition in $La_{1-x}Sr_xVO_3$. In: *Phys. Rev. B* **52**, R2213(R) (1995).

[9] S. Miyasaka, J. Fujioka, M. Iwama, Y. Okimoto, and Y. Tokura: Raman study of spin and orbital order and excitations in perovskite-type RVO_3 (R=La, Nd, and Y). IN: *Phys. Rev. B* **73**, 224436 (2006).

[10] S. Miyasaka, T. Okuda, and Y. Tokura: Critical behavior of metal-insulator transition in $La_{1-x}Sr_xVO_3$. In: *Phys. Rev. Lett.* **85**, 5388 (2000).

[11] S. Miyasaka, S. Onodo, Y. Okimoto, J. Fujioka, M. Ywama, N. Nagaosa, and Y. Tokura: One-dimensional orbital excitations in vanadium oxides. In: *Phys. Rev. Lett.* **94**, 076405 (2005).

[12] D.L. Proffit, H.W. Jang, S. Lee, C.T. Nelson, X.Q. Pan, M.S. Rzchowski, and C.B. Eom: Influence of symmetry mismatch on heteroepitaxial growth of perovskite thin films. In: *Appl. Phys. Lett.* **93**, 111912 (2008).

[13] L.G. Quagliano and Zbig Sobiesierski: Raman scattering as a probe of the tensile strain distribution in GaAs grown on Si(111) by molecular beam epitaxy. In: *Superlattices and Microstructures* **13**, 0749-6036 (1993).

[14] B. Roberge, S. Jandl, A.A. Nugroho, T.T.M. Palstra, L.D. Tung, and G. Balakrishnan: Study of phase coexistence in YVO_3 and $LaVO_3$. In: *J. Raman Spectrosc.* **46** 1157 (2015).

[15] H. Rotella, U. Lüders, P.-E. Janolin, V.H. Dao, D. Chateigner, R. Feyerherm, E. Dudzik, and W. Prellier: Octahedral tilting in strained $LaVO_3$ films. In: *Phys. Rev. B* **85**, 184101 (2012).

[16] M. Schmidbauer, A. Kwasniewski, and J. Schwarzkopf: High-precision absolute lattice parameter determination of $SrTiO_3$, $DyScO_3$ and $NdGaO_3$ single crystals. In: *Acta Cryst.* **B68**, 8-14 (2012).

[17] G. Sclauzero and C. Ederer: Structural and electronic properties of epitaxially strained $LaVO_3$ from density functional theory and dynamical mean-field theory. In: *Phys. Rev. B* **92**, 235112 (2015).

[18] S. Sugai and K. Hirota: Orbital waves in YVO_3 studied by Raman scattering. In: *Phys. Rev. B* **72**, 020409(R) (2006).

[19] I. Vrejoiu, C. Himcinschi, L. Jin, C. Jia, N. Raab, J. Engelmayer, R. Waser, R. Dittmann, and P.H.M. van Loosdrecht: Probing orbital ordering in $LaVO_3$ epitaxial films by Raman scattering. In: *APL Mater.* **4**, 046103 (2016).

[20] `http://bwtek.com/raman-theory-of-raman-scattering/`, access 06.04.2016.

[21] `http://www.physik.fu-berlin.de/studium/praktika-forward/fpa_dipl-ws2009/docs/Ma7_Raman.pdf`, access 06.04.2016.

List of Figures

Statutory Declaration/Eidesstattliche Erklärung

Hiermit versichere ich an Eides statt, dass ich die vorliegende Arbeit selbstständig und ohne die Benutzung anderer als der angegebenen Hilfsmittel angefertigt habe. Alle Stellen, die wörtlich oder sinngemäß aus veröffentlichten und nicht veröffentlichten Schriften entnommen wurden, sind als solche kenntlich gemacht. Die Arbeit ist in gleicher oder ähnlicher Form oder auszugsweise im Rahmen einer anderen Prüfung noch nicht vorgelegt worden. Ich versichere, dass die eingereichte elektronische Fassung der eingereichten Druckfassung vollständig entspricht.

Place and Date, Signature

Acknowledgement

To all who have supported me during the last months, I would like to express my sincere gratitude; most importantly, to Dr. Ionela Lindfors-Vrejoiu for supervision, valuable feedback and being my key reference person. Dr. Lindfors-Vrejoiu has also produced the samples used in this study. Furthermore, I have to thank Dr. Cameliu Hincinschi and also his colleagues for giving me the opportunity to carry out the Raman measurements in their laboratory at the TU Bergakademie Freiberg. Working there and in the lab in Cologne as well taught me a lot about experimental work. For this, I thank my colleagues from Cologne, Dr. Thomas Koethe and especially Raphael German, who never showed impatience when difficulties came up. Finally, my thank goes also to Prof. Dr. Paul van Loosdrecht for giving me the opportunity to learn a lot by working in his group. I am confident that all the other poeple to whom I am obliged will know who I am referring to.